JJMIE

Volume 18, Number 2, June. 2024
ISSN 1995-6665
Pages 339- 350
https://doi.org/10.59038/jjmie/180207
Editor-in-Chief: Prof. Ali M. Jawarneh

Jordan Journal of Mechanical and Industrial Engineering

# Preparation and Exploration of Nano-Multi-Layers on 316l Stainless Steel for Surgical Tools

Ali Hubi Haleem[1], Nabaa Sattar Radhi[1*], Nada Talib Jaber[1,2], Zainab Al-Khafaji[3,4]

[1] University of Babylon/Department of Metallurgy Engineering/Babylon, Iraq.

[2] Republic of Iraq / Al-Qadissyia government / Department of Planning and Strategic Development

[3] Imam Ja'afar Al-Sadiq University, Qahira, Baghdad, Iraq.

[4] Department of Civil Engineering, Faculty of Engineering and Built Environment, University Kebangsaan Malaysia, 43600 UKM Bangi, Selangor, Malaysia.

Received 30 Sep 2023 Accepted 10 Mar 2024

**Abstract**

Biocompatibility and tribological issues with 316L stainless steel (SS) biomaterials reduce their service life. A metallic substrate made of stainless steel 316L (SS) was employed. After being subjected to a surface anodization process using sulfuric and nitric acids, it was coated with silver using a DC sputtering plasma method. The coating's crystallinity, morphology, and microstructure have been investigated using structural characterization methods such as XRD, FESEM, and EDS. To assess the coatings' qualitative adherence to the steel substrates, the coated substrates underwent the Rockwell - C indentation tests. An optical profilometer was used to measure the coatings' surface properties. The corrosion resistance of coated and uncoated SS substrates was evaluated using potentio-dynamic polarization experiments. The results show that the silver coating and anodized surface increase SS's resistance to corrosion behavior. The silver-coated SS and surfaces treated for corrosion both see a reduction in the current density of corrosion. These further demonstrate the potential for using surface-treated and silver-coated stainless steel as a surgical instrument to increase biocompatibility and resistance to corrosion.



**Keywords:** 316L biomedical stainless steel; anodization; DC sputtering; hardness; coating thickness; rough-ness and corrosion rate.

## 1. Introduction

Only a select few biocompatible metals and alloys can function as durable orthopedic medical implants over an extended period. Stainless steel 316L, cobalt-chromium alloy, titanium, and Ti–6Al–4 V alloy are frequently utilized as bone fixators in hip prostheses and knee, external fixators, dental implants, and orthodontic wires [1]–[4]. Stainless steel (316L) is often used in orthopedic procedures because of its strong mechanical properties, flexibility, high resistance to breaking, and cost-effectiveness [5]–[10]. SS316L implants experience pitting corrosion in the bodily fluid environment, leading to the need for device removal in some instances [11]. Stainless steel is prone to corrosion in low-oxygen environments and gaps where the protective passive coating is compromised. These implants, like the femoral components, might fail owing to fractures. Another limitation of SS-316L in biomedical uses is its poor tissue integration and low blood compatibility due to allergic reactions caused by its nickel presence. Various bioactive coatings, including nHA-PLA composite, 45S5 bioglass-silica, polysiloxane/bioactive glass composite, phosphate-free bioactive glass [12], Mg-substituted fluorapatite, Ce integrated Nb2O5 composite, and organosilicon thin films, have been applied. Utilizing Fe-based alloy on SS316L may help achieve prompt biological attachment, reduce corrosion, and address small placement problems in metallic prostheses after surgery [13]–[19].

DC Sputtering is a PVD Coating method in which a target material is attacked with ionized gas molecules, causing atoms to be ejected into the plasma. The vaporized atoms are deposited as a thin layer on the substrate when they condense. DC Sputtering is a fundamental and cost-effective method used for Physical Vapor Deposition (PVD) of metal for covering electrically conductive target materials [18], [20], [21]. DC is advantageous as a power source for this process due to its controllability and cost-effectiveness, especially for metal deposition in coating applications. DC Sputtering is frequently utilized in the semiconductor industry to produce microchip circuits at the molecular scale. It is used for gold sputter coatings on jewelry, watches, ornamental finishes, non-reflective glass, optical components, and metalized packaging plastics.

There are many types of sputtering, including DC Sputtering and RF. Magnetron sputtering, etching plasma sputtering, and Ion beam sputtering [22]. Direct current sputtering (DC sputtering) is the simplest of these systems.

* Corresponding author e-mail: mat.nabaa.sattar@uobabylon.edu.iq.

 

That was used in this research. The Sputtering system consists of two plates, a vacuum chamber, and a pair of planar electrodes; the material to be deposited in the cathode, the anode is where the substrates are located. The sputtering chamber contains Ar and $O_2$ discharge gas [23]. Anodization has been used to improve corrosion resistance in several research [24].

Silver may be added into or coated on polymers or metals using techniques such as lyophilization [25], [26], dip coating [27], electrospinning [28], [29], layer-by-layer deposition [30], and additive manufacturing [31]. These approaches show significant possibilities for using silver to improve the antibacterial properties of biomaterials [32]–[35]. The metal surface of the anode is coated with a passive layer by an electrolytic process known as anodization. In an oxygen-rich environment, anodized metals may form a thin oxide coating. A thick and uniform layer of anodized oxide limits ionic conductivity. Therefore, these oxides can be considered barriers that keep the metal from corroding anymore [36].

The novelty of current research was focused on using a multi-coating layer; two coating processes were adopted sequentially (chemical process first and then physical process) presented by anodization (precipitated layer of $Cr_2O_3$) and DC sputtered plasma (Nano-Ag), respectively. The main objective of using Nano-Ag was to minimize the porous generated during the creation of $Cr_2O_3$. Using a multi-coating layer by hybrid process (chemical and physical processes) improved the corrosion resistance in Tyrode's solution at 37±1 degree centigrade. This study aimed to improve surgical tools' biocompatibility, adhesion, and corrosion behavior by using the anodization and DC sputtered plasma of silver coating on 316L SS, depending on international standards after exposure to the physiological Tyrode solution.

## 2. EXPERIMENTAL WORK

The chemical composition of the stainless steel (316L), which was cut into samples measuring 15 mm in diameter and 3 mm in height for the tests, is illustrated in Table 1. The test sample was cleaned by immersing it in an ultrasonic cleaner for ten minutes in each of ethanol and acetone, followed by drying. The negative electrode for the anodization procedure was made of silver (2 1 0.03) cm, while the positive electrode was made of stainless steel. During the anodization process, a 4 cm gap existed between the two electrodes. The electrolyte was a solution comprising 1M H2SO4 and 1M HNO3 that was kept at a constant temperature of 25° C.

The test specimen had been subjected to anodization voltage increases of 6, 8, and 10 volts for durations of 5 and 10 minutes, respectively. Following anodization, the test piece was cleaned with distillate and dried.

The most valuable specimen was then covered with silver utilizing a DC sputtering plasma, and the specimen was inserted into the PVD system's deposition chamber as shown in Figure 1. The temp was then set when the chamber was evacuated to a base pressure of less than $1x10^{-3}$ torr. Ensuring an equal $O_2$/Ar oxygen flow and an operational pressure of 6 x $10^{-2}$ torr (0:10). The working voltage and electrical current in this work are 1400V and 20 mA, respectively. Two hours were spent on the deposit. The test sample's surface was then heat-treated for a total of 60 minutes at a temp of 400 ° C following the coating procedure.

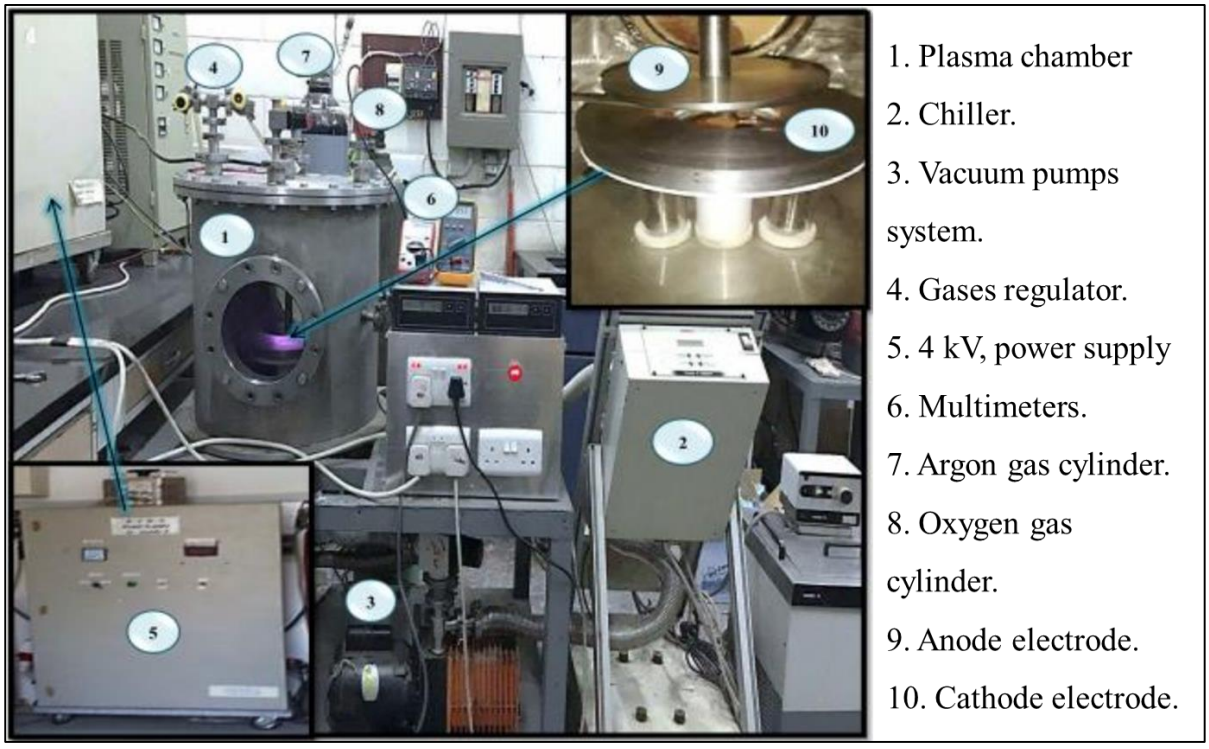


**Figure 1.** DC Sputtering plasma system set-up

## 3. Tests

The structural analysis and observation of the structural form of the oxide film on the surface of the stainless steel applied throughout the anodization process and sputtered specimen were conducted using field-emission scan electrons microscopy (FE-SEM) and EDS [37]. The samples have been ground on edge while holding the specimen vertically to examine the cross-sectional photographs. Atomic force microscopy (AFM) was used to measure the extended surface topography. Using an X-ray diffractometer (XRD), the phase and crystallographic structure of the thin film has been determined and investigated. The corrosion behavior was then evaluated using a potentiodynamic polarization (PDP) test. The test sample was immersed in a Tyrode solution and then measured. Three electrodes were utilized in the test: the test sample served as the working electrode, platinum (Pt) served as the counter electrode, and the saturated calomel electrode (SCE) served as the reference electrode. A conventional Rockwell hardness tester equipped with a Rockwell (such as the kind - C) diamond cone weighing (150 kg) at 2 seconds was utilized for the Rockwell-C adhesion test. The indented classes ("HF1" and "HF2") indicate adequate adherence. The inhibition zone approach is used to investigate antibacterial activity. An antibacterial kinetic test using gram-negative "E. coli" strains (Escherichia coli, American kind culture, "ATCC 5922").

## 4. RESULTS AND DISCUSSIONS

The XRD spectra for the anodized specimen at improved voltage 8V for 5 minutes are shown in Figure 2. Unmistakably, the anodized sample displayed the usual austenite (γ) phase reflection peaks. On the anodized specimen, nevertheless, it was discovered that the reflection peaks for chromium oxide $Cr_2O_3$ were present.

Figure 3 shows the XRD pattern of the substrate 316L stainless steel and as-sputtered Ag thin scale of the anodized sample. An index of the diffraction rings can be determined from the d-spacing calculation (111), (002), (022), (113), and (222) for Ag.

### *4.1. Film Composition and Coating Morphology*

Figure 4 shows an optical microscope of surface microstructure of 316l stainless steel and Figure 5 shows an optical microscope of surface microstructure anodized 316l at different voltage and time. The surface is made up of porous that appear at higher magnification of 400X. A considerable increase in the mechanical characteristics, including microhardness, is shown in the optical micrograph of the specimens that have been anodized at a thickness of 4 cm. It is clear from the optical microscopy of this set of specimens that the anodizing processes were successful given the high porosity, appropriate pore geometry, and suitable anodizing procedure.

**Table 1.** Chemical Composition of the Alloy utilized in this research

| Material | Cr | Ni | Mo | P | Mn | Cu | Al | S | Si | C | Fe |
|---|---|---|---|---|---|---|---|---|---|---|---|
| % Weight | 17 | 10.36 | 2.37 | 0.023 | 1.36 | 0.185 | 0.004 | 0.029 | 0.813 | 0.03 | Bal. |

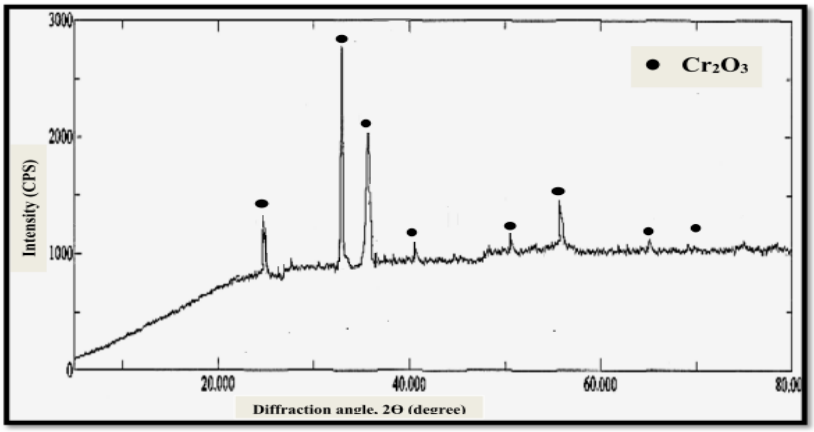


**Figure 2.** X-ray diffraction pattern of anodized sample at 6v, 5min

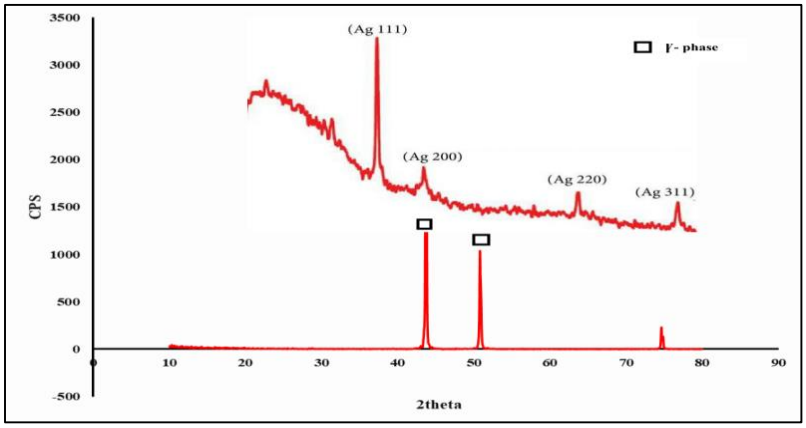


**Figure 3.** XRD profiles of the 316L stainless steel and sputtered sample at 2hr.

 

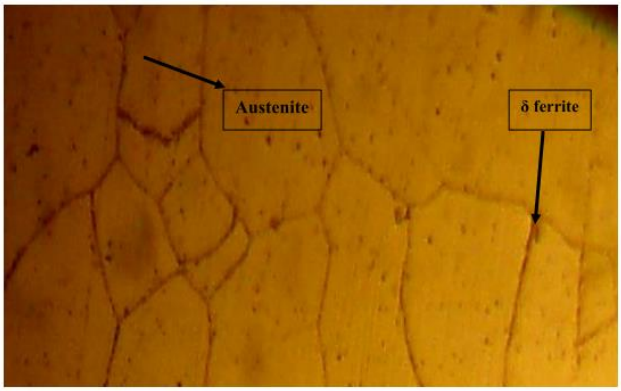


**Figure 4.** OM morphology of 316l stainless steel.

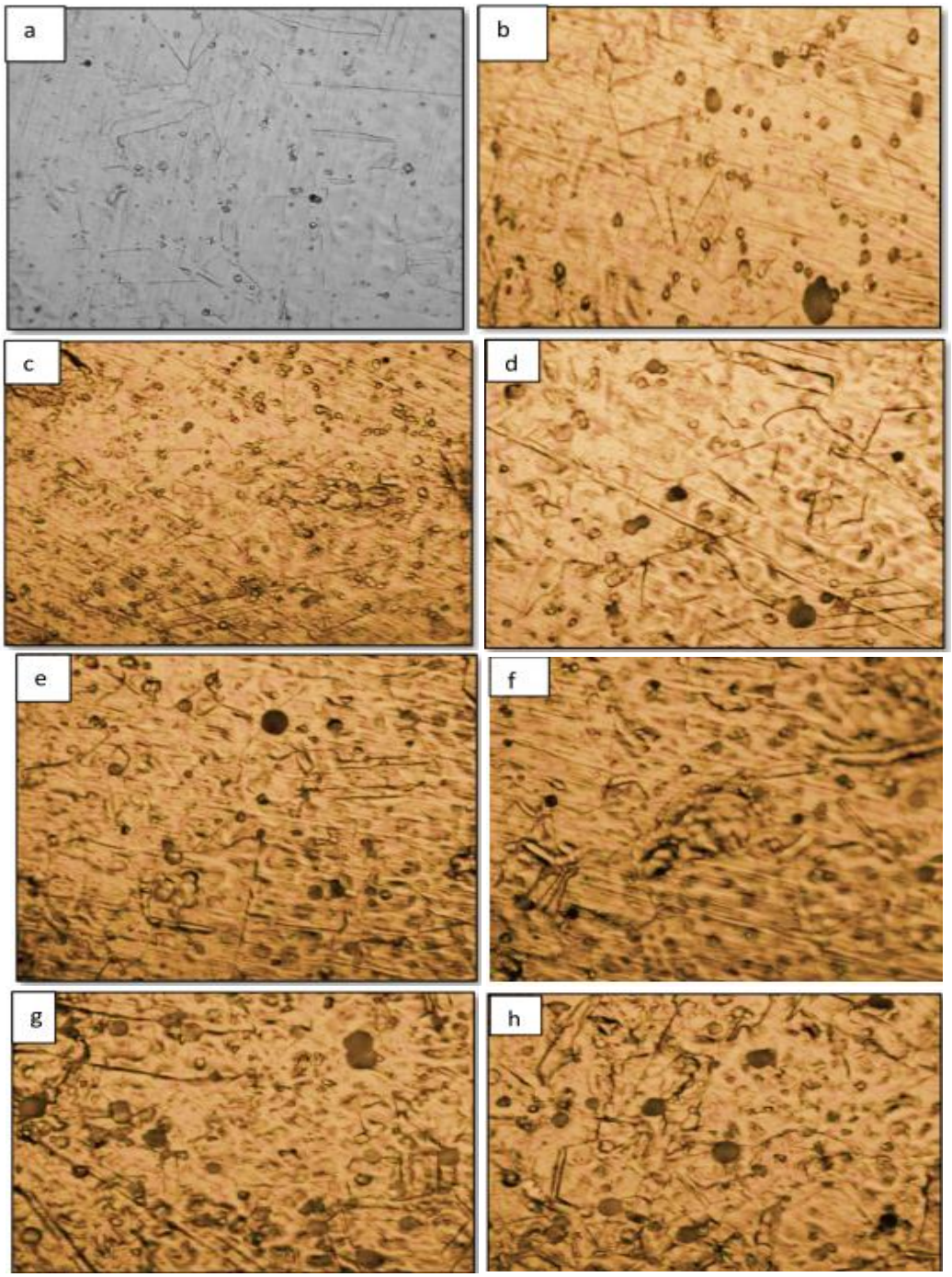


**Figure 5.** OM morphology of an anodize 316l alloy surface (at 4 cm e: 6 V,5min, f: 6 V,10 min, g: 8 V,5min, h: 8 V,10min).

*4.2. Corrosion Behavior*

*4.2.1. Polarization Tests*

Figure 6 display the potentiodynamic polarization detour of base 316L SS and samples that have been anodized in the Tyrode's solution at a range of temperatures at 37°C for a different time. The corrosion current ($i_{corr}$) and (Ecorr) are obtained from the potentiodynamic curving by employing a Tafel plot and they are recorded in tables (2). It is evident from the findings in the tables, the unmodified substrate has ($i_{corr}$= 0.44 µA), caused by the dissolution of metallic ions on the external surface of the unmodified base, it has the lowest corrosion resistance.

After anodization, corrosion current in anodized samples is seen to decrease for (A24, A34, A44, and A54), This means that the anodization process provides a barrier to corrosion on the substrate's exposed surface. the lowest corrosion current achieved during anodization at 8 V, 5 minutes ($i_{corr}$ = 0.112 µA) resulted in higher corrosion resistance than anodization at 10 V. This is because of the extremely compact structure of this oxide layer. In addition, the anodization at a higher potential produced turbulence in the electrolyte, leading to a rough and inadequate surface.

Figure 7 shows the potentiodynamic polarization curves for base 316L SS alloy, anodized sample A34, and sputtered sample with Ag in the Tyrode's solutions at 37 ±1 °C. The current of the corrosion is ($i_{corr}$) and the potentials of corrosion (Ecorr) are derivative from the potentiodynamic curving by employing the Tafel plot (Table 3). Table 3 demonstrates the obtained results, the unmodified sample has corrosion current ($i_{corr}$= 0.44 µA), the sputtering with time (2 hrs), this time-treated sample shows better corrosion resistance than the untreated sample. This indicates that sputtering with an Ag coating layer would create a passive layer of protection on the surface that would slow the percentage of corrosion. After sputtering at 2 hrs, the lowest ($i_{corr}$= 0.085 µA) is found and this consequence has the maximum corrosion resistance.

*4.3. Cyclic Polarization*

Cyclic polarization is performed to examine the sample's resistance to localized corrosion. Figure 8 illustrates the cyclic polarization curve for an anodized sample at 8 volts, 5 min, 4 cm, and sputtered sample at 2 hrs. For anodized sample, has Epit ≈ Eprot little tendency to pit. The cyclic polarization curves obtained as noted in Table (4), the extent of the hysteresis loop is highly reduced and therefore, the corrosion mechanism operating on the substrate surface is less active when coating with silver. the ΔE rate obtained is low and consequently, the pitting corrosion resistance of this specimen would be higher. Coating of Ag increases resistance to pitting corrosion of anodized 316l St-St.

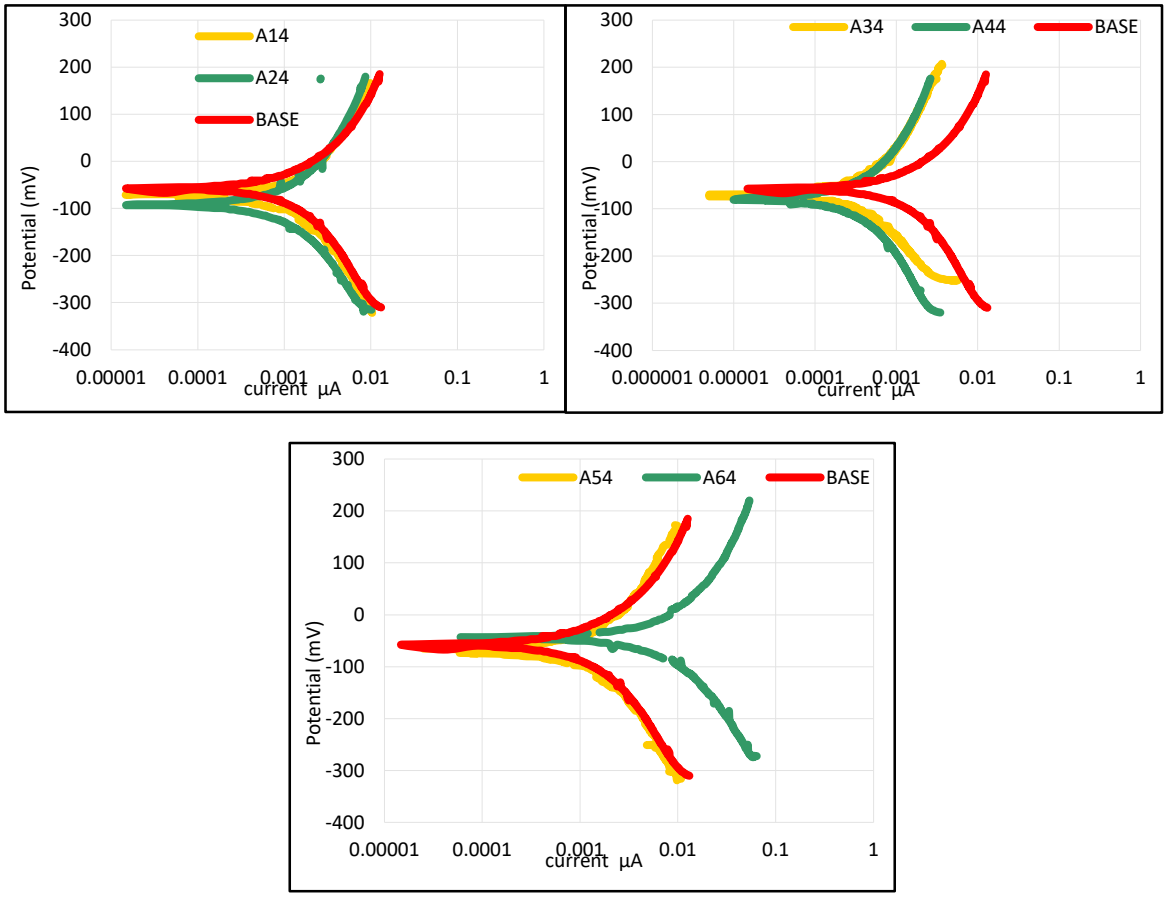


**Figure 6.** Potentiodynamic Polarization for 316l Alloy in Tyrode's solution (A14: 6 volts, 5min, A24: 6-volt, 10 min, A34: 8volt, 5min, A44: 8volt, 10 min, A54: 10volt, 5min, A64: 10 volts, 10min).

 

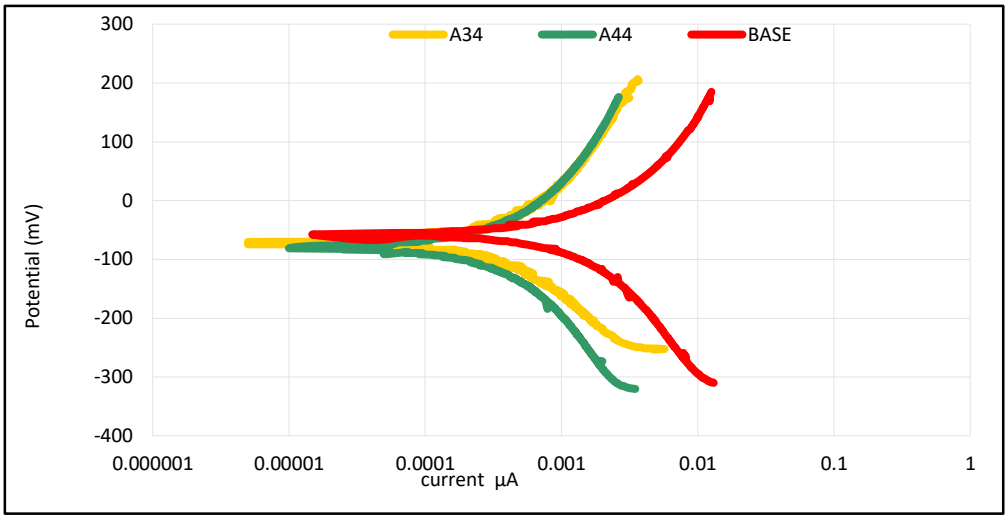


**Figure 7.** Potentiodynamic polarization curves of base 316L and sputtered sample with Ag of the anodized sample at (8 V, 5min, and 4cm).

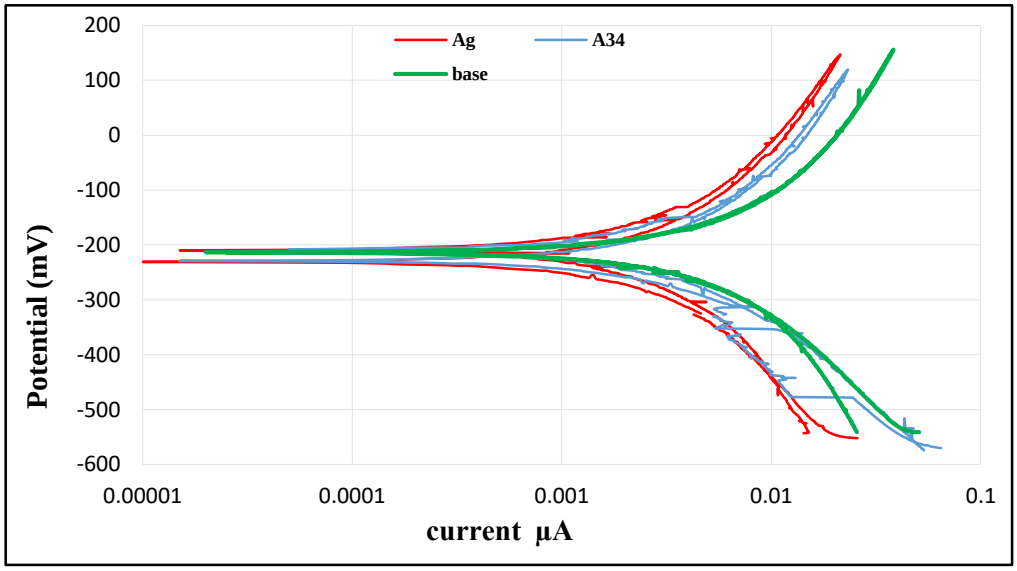


**Figure 8.** Cyclic polarization curves for anodized and sputtered samples in Tyrode's solution at 37 ±1 °C.

**Table 2.** Electrochemical parameters of the anodized samples for 316L SS at different parameters at 4cm.

| **Sample code** | **Conditions** | $i_{corr}$. **µA** | **CR (mpy)** | **Improvement Percentage%** |
|---|---|---|---|---|
| **Base** | **Untreated** | 0.44 | 0.1033 | - |
| **A14** | 6V, 5min | 0.412 | 0.0967 | 6 |
| **A24** | 6V, 10min | 0.336 | 0.0788 | 24 |
| **A34** | 8V, 5min | 0.112 | 0.0262 | 75 |
| **A44** | 8V, 10min | 0.130 | 0.0305 | 70 |
| **A54** | 10V, 5min | 0.681 | 0.1598 | - |
| **A64** | 10V, 10min | 2.28 | 0.5353 | - |

**Table 3.** Electrochemical parameters of the sputtered sample with Ag for anodized 316L SS.

| Sample code | Conditions | $i_{corr}$. µA | Ecorr.mV | CR (mpy) | Improvement % |
|---|---|---|---|---|---|
| Base | Untreated | 0.44 | -56.7 | 0.1033 | - |
| A34 | 8volt, 5min | 0.112 | -66.8 | 0.0262 | 75 |
| Ag | DC sputtering | 0.085 | -72.9 | 0.0199 | 81 |

**Table 4.** pitting potential values of anodized and sputtered samples with Ag.

| Sample code | Conditions | Ep (mV) | **Eprot**. (mV) | ΔE=(**Epit-Eprot**.) (mV) |
|---|---|---|---|---|
| Ag | DC sputtering | -150 | -90 | -60 |
| A34 | 8volt, 5min, 4cm | -140 | -150 | 10 |

*4.4. EDS*

Figure 9 shows the morphological features of the 316L SS surface modified by anodization process at 8 V for 5min time at 4cm distance. The figure reveals the formation of a homogeneously distributed oxide scale with a nano porous structure. The dual porous structure was related to the anodic voltage. Figure 10 demonstrates the EDS analysis of the 316L SS surface modified by anodization process at 8 V ,5 min. The results confirm the formation of $Cr_2O_3$ oxide scale in the treated sample due to existence of Cr and O elements as major constituents of $Cr_2O_3$. Interfaces can be seen clearly between sputtered scale and substrate. The element distribution in sputtered silver samples is depicted in Figure 11 which is O, Cr, and Ag which match with EDS analysis.

*4.5. Atomic Force Microscopy Analysis*

The AFM analysis is done for the anodized alloy and the topography of the anodized sample with 3D performance images were shown in Figure (12). The topography shows a compact and regular scale of the anodized 316L, as well as the surface roughness, which was (11.7) nm. The illustrated topography indicates that the surface of the anodized sample is covered by semispherical $Cr_2O_3$ particles. The AFM analysis is done for the sputtered sample and the topography of the surface with 3D performance images shown in Figure (13) features a topography that, while not particularly rough, does have several peaks and valleys which is a characteristic feature for as-deposited scales. The as-deposited sample has a very low roughness because of the uniform sputtering.

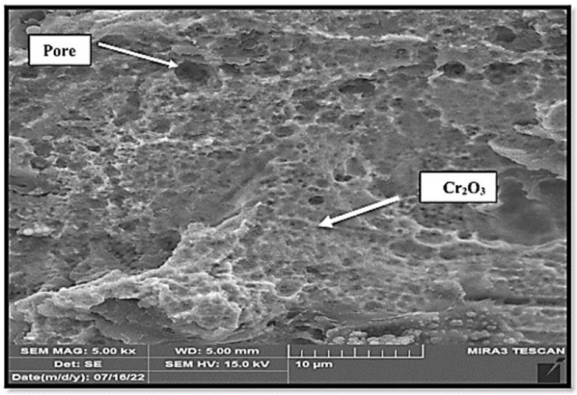


**Figure 9.** demonstrates the EDS analysis of the 316L SS surface modified by the anodization process at 8 V,5 min. The results confirm the formation of the $Cr_2O_3$ oxide scale in the treated sample.

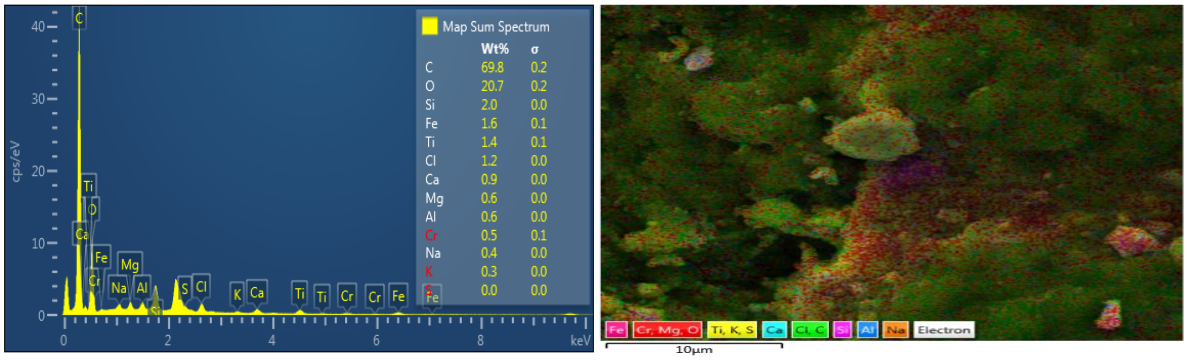


**Figure 10.** EDS analysis for anodized samples at 8volt, 5min, and 4cm.

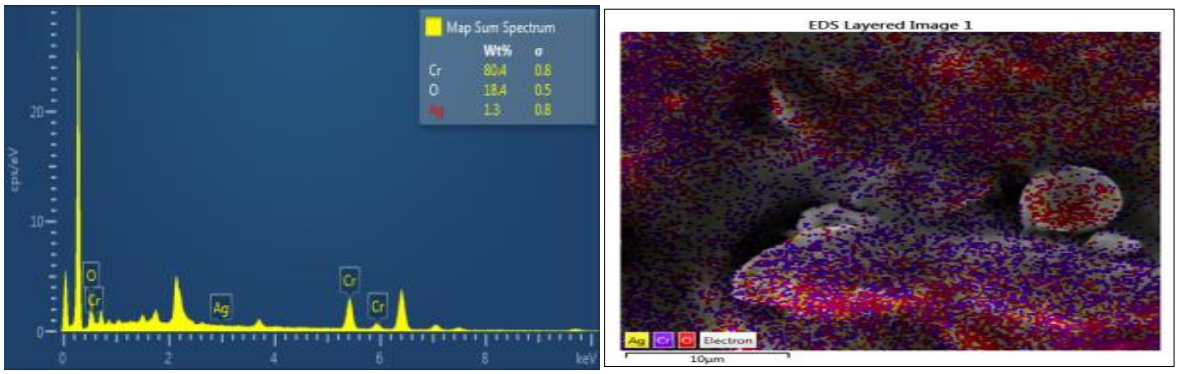


**Figure 11.** EDS analysis for a sputtered sample at 2hr.

 

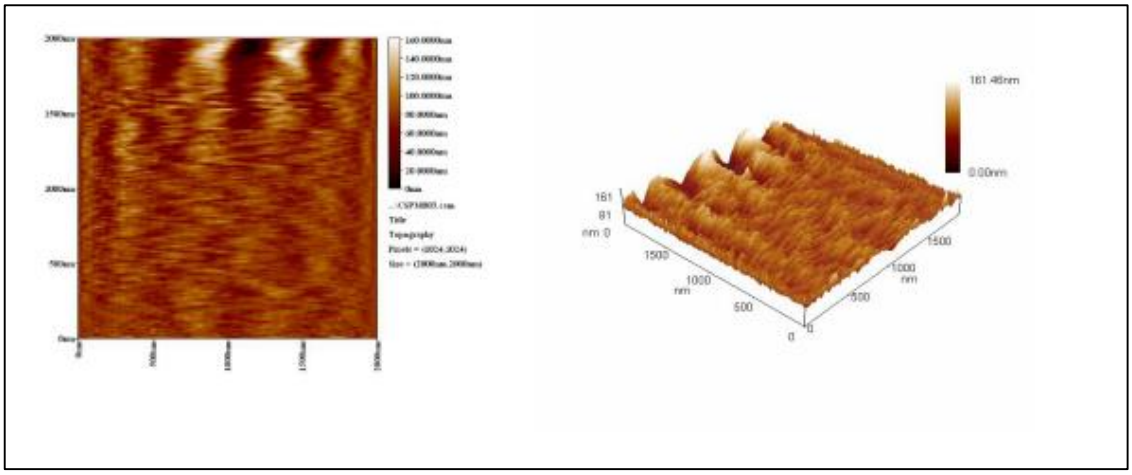

**Figure 12.** The topography of the anodized samples with 3D performance images at 8 volts, 5min, 4 cm.

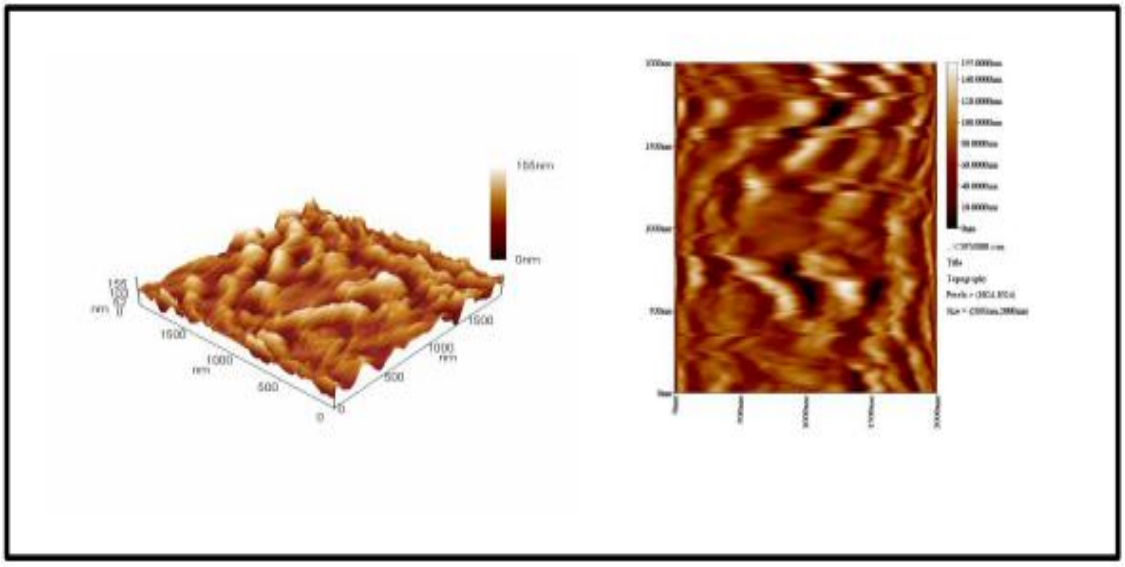

**Figure 13.** The topography of the sputtered sample with 3D performance images.

*4.6. Adhesion Test*

Figure (14) shows the optical microscope (OM) images of Rockwell- C indentations on the anodized 316L. When an indentation was made in an anodized sample, cracks both deep and long appeared around the indentation. Not only that but didn't find any delamination near the indentation and made it with a Rockwell C scale. These findings demonstrate the quality and strength of the adhesion of this sample are correlated to HF1 and HF2 and these failures represent HF2–HF3 type of adhesion strength quality.

Figure 15 shows the Optical microscope (OM) images of Rockwell C indentation with three different magnifications (5X, 10X, 20X) on the sputtered samples with Ag. At a deposition time of 2 hours, shallow, short cracks can be seen developing around the deformation point in Ag sputtering samples. Delamination also does not occur near the area of the Rockwell - C indentation effect. Each of these scales only has tiny cracks inside the indentation. The sample has an HF ranking of 1 that indicates silver scale and coating done by sputtering in this work show good adhesion. Miniscule cracking in the coating demonstrated strong adhesion to the base material.

*4.7. Field Emission Scanning Electron Microscopy.*

Figure 16 reveals 316L stainless steel's distinctive structure modified by the anodization method at 8 Volt for 5min at a 4cm distance. In the image, can see the development of a nano porous oxide scale that has spread uniformly. The dual porous structure was related to the anodic voltage. Figure 17 shows a typical FESEM cross sections morphology of the oxide scales on the anodized steel for 5min at 8volt and 4cm. The anodized films grew to a very uniform thickness across the surface. The morphology and topography of sputtered sample with Ag were observed by FSEM in Figure (18). The FSEM surface micrograph shows a smoother surface. The microstructure is uniformly packed, and the particles are evenly distributed, which results in uniform coatings. Figure 18 illustrates the cross-sectional topography of sputtered sample with Ag at 2 hrs. The sputtered scale is regular in its thin-scale structure, measuring in at a thickness of 89.05 nm, and demonstrates improved compactness, homogeneity, and full bond strength between both the substrate and the coating.

*4.8. Antibacterial Test*

The effect of the antibacterial for 316L, anodized 316L SS alloy, and sputtered samples were tested against an E. coli culture, as can be seen in (Figure 19). The oxide scale exhibited a strong antibacterial effect. Therefore, the presence of $Cr_2O_3$ was effective in inhibiting bacterial attachment to the surface due to its surface roughness, which in turn inhibits bacterial growth and enhances antibacterial properties. For sputtered samples, it has shown the highest antimicrobial activity, this refers to Ag coating's active role in killing bacterial strains.

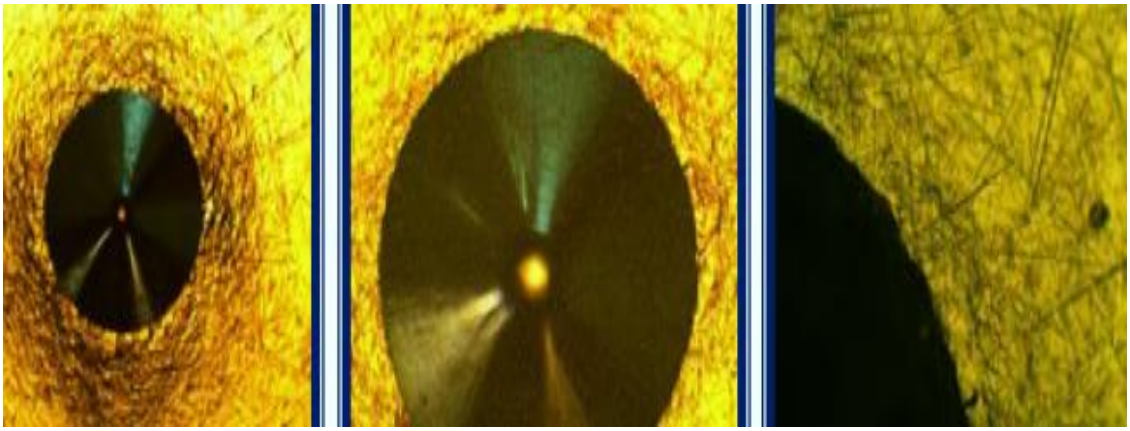

**Figure 14.** Rockwell type-C causes an indentation in an anodized specimen at 8volt, 5min, and 4cm.

**Figure 15.** Rockwell type - C test for sputtered samples with Ag at 2 hrs.

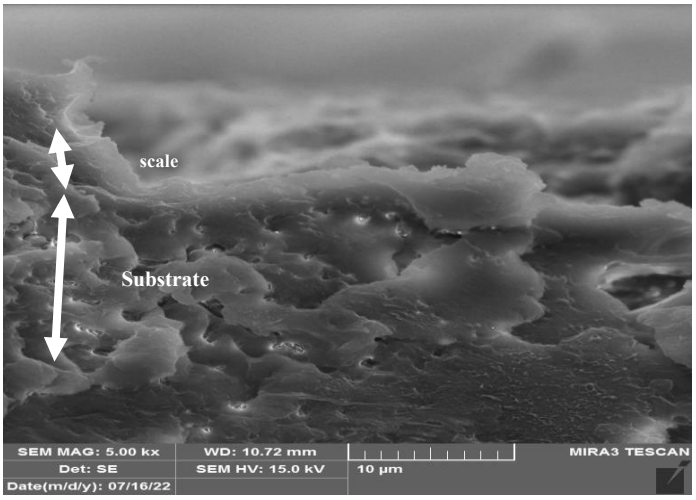


**Figure 16.** FESEM cross sections morphology of the anodized sample.

 

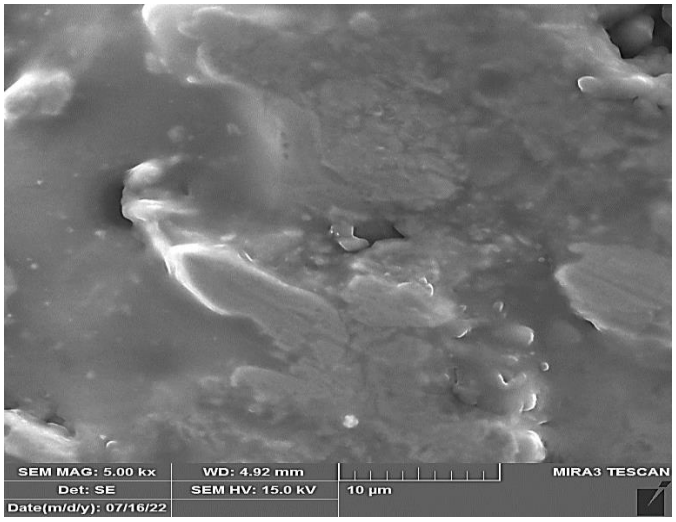


**Figure 17.** FSEM micrographs of silver coating on anodized 316L SS alloy at 2 hrs.

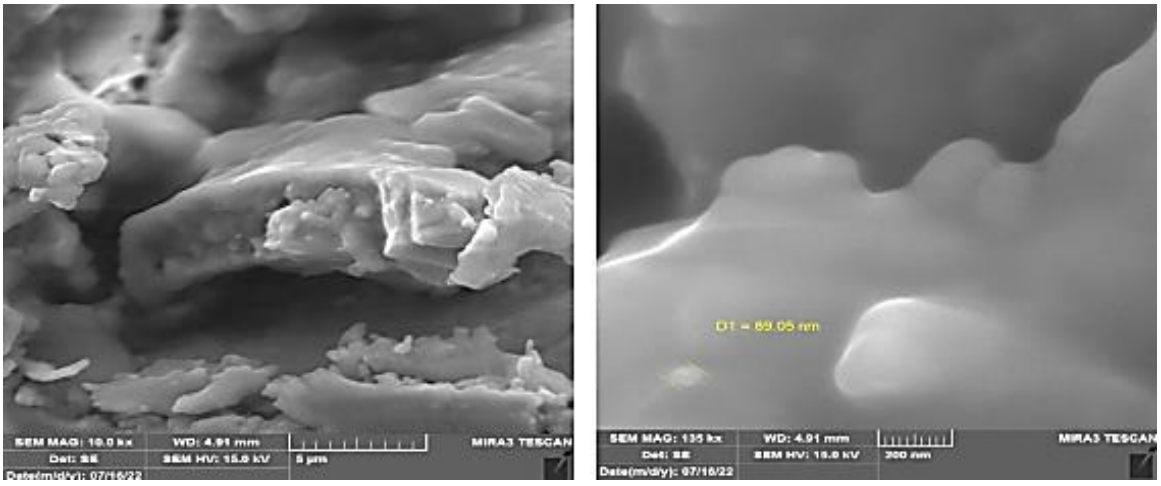


**Figure 18.** FESEM cross sections morphology of the sputtered sample.

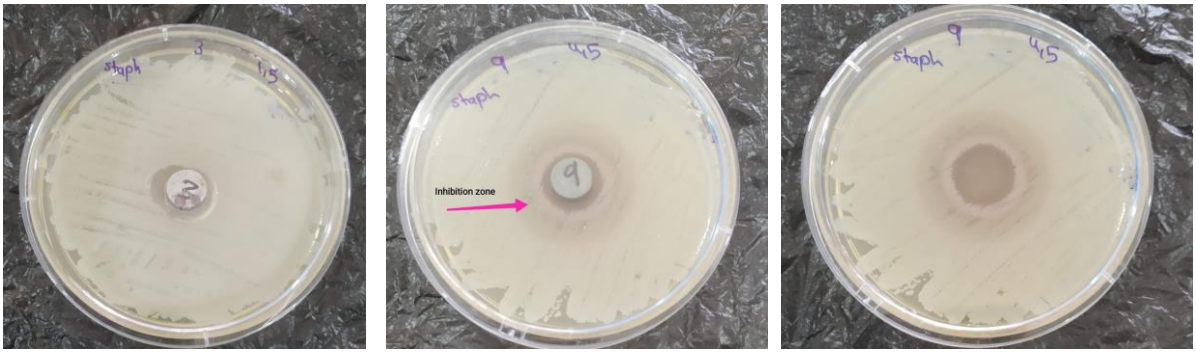


**Figure 19.** Antibacterial Test.

## 5. CONCLUSIONS

Nanoporous structures of $Cr_2O_3$ in different morphologies are obtained by tailoring the major anodization parameters of applied potential, distance, and time. The main anodization parameters of applied voltage, distance and time have a significant effect on the corrosion resistance of anodized sample is produced throughout anodization process of 8V, 4Cm and time of 5 min.

- XRD analysis reveals the formation of several sharp and strong intense peaks attributed to anatase $Cr_2O_3$ along with one diffraction peak corresponding to rutile $Cr_2O_3$ in the anodized 316L substrates at 8V, 4Cm and time of 5 min.
- The major anodization parameters of applied voltage, distance and time have an obvious influence on the thickness of formed $Cr_2O_3$ as it increases with increasing these parameters. Here, 316L substrates anodized at voltage of 8V at 4cm for 5 min had the highest thickness compared to other anodized samples.
- The values of the surface roughness of anodized 316L substrates increase evidently compared to non-anodized 316L sample. The surface roughness increased, when the applied voltage, distance and time were at values 8 V, 4Cm and 150 min, respectively.

- The electrochemical results displayed that the 316L samples anodized at 6 and 8 V have an inferior corrosion behavior compared to that of the non-anodized 316L sample. The increase of the applied potential from 6 to 8 V had a significant effect on the corrosion behavior. The results confirmed that the protective anodized $Cr_2O_3$ layer formed onto 316L surface at 8 V for 5 min is more stable compared to that formed at 6, resulting in further preventing from corrosion effect.
- The morphology of the sputtered Ag layer is homogenous and crack-free when sputtered, with the optimum time at 2 hrs.
- The potentiodynamic and cyclic polarization results demonstrate that the DC sputtering plasma method on 316L SS at 2 hrs. has highest corrosion resistance, and an improvement in the pitting corrosion resistance when immersed in the Ringer's solution.
- Adhesion strength results for modified samples compared with nonmodified samples appear to be good adhesive for the anodized and sputtered deposited layers with Ag on 316L substrate.
- The results of antibacterial analysis have confirmed that the DC sputtered coating by Ag reveal good antibacterial activity against gram negative E. coli. This antibacterial activity increases when surface treatment time increases. That makes these coatings safe, and they can be used for surgical instruments applications.

## REFERENCES


[1] H. A. Sallal *et al.*, "Effect of adding (ZrO2-ZnO) nanopowder on the polymer blend (lamination and methyl vinyl silicone) in a hybrid nanocomposite material," *Journal of King Saud University-Science*, vol. 36, no. 2, p. 103061, 2024.

[2] A. Al-Bashir, A. K. A. Jawwad, and K. A. Shgair, "Evaluating the effects of high velocity oxy-fuel (HVOF) process parameters on wear resistance of steel-shaft materials," *Jordan Journal of Mechanical and Industrial Engineering*, vol. 3, no. 2, 2009.

[3] A. R. I. Kheder, N. M. Jubeh, and E. M. Tahah, "Fatigue Properties under Constant Stress/Variable Stress Amplitude and Coaxing Effect of Acicular Ductile Iron and 42 CrMo4 Steel.," *Jordan Journal of Mechanical and Industrial Engineering*, vol. 5, no. 4, 2011.

[4] R. Das, M. K. Pradhan, and C. Das, "Prediction of surface roughness in Electrical Discharge Machining of SKD 11 TOOL steel using Recurrent Elman Networks," *Jordan Journal of Mechanical and Industrial Engineering*, vol. 7, no. 1, 2013.

[5] A. H. Jasim, N. S. Radhi, N. E. Kareem, Z. S. Al-Khafaji, and M. Falah, "Identification and investigation of corrosion behavior of electroless composite coating on steel substrate," *Open Engineering*, vol. 13, no. 1, p. 20220472, 2023.

[6] K. M. Abed, N. S. Radhi, A. H. Jasim, Z. S. Al-Khafaji, S. Radhi, and S. A. Hussien, "Study the effect of adding zirconia particles to nickel–phosphorus electroless coatings as product innovation on stainless steel substrate," *Open Engineering*, vol. 12, no. 1, pp. 1038–1045, 2022, doi: 10.1515/eng-2022-0364.

[7] N. D. Fahad, N. S. Radhi, Z. S. Al-Khafaji, and A. A. Diwan, "Surface modification of hybrid composite multilayers spin cold spraying for biomedical duplex stainless steel," *Heliyon*, 2023, doi: 10.1016/j.heliyon.2023.e14103.

[8] S. Sattar, Y. Alaiwi, N. S. Radhi, and Z. Al-khafaji, "Numerical Simulation for Effect of Composite Coating ( TiO2 + SiO2 ) Thickness on Steam Turbine Blades Thermal and Stress Distribution," *ACADEMIC JOURNAL OF MANUFACTURING ENGINEERING*, vol. 21, no. 4, 2023.

[9] S. Sattar *et al.*, "Corrosion reduction in steam turbine blades using nano-composite coating," *Journal of King Saud University-Science*, vol. 35, no. 8, p. 102861, 2023, doi: 10.1016/j.jksus.2023.102861.

[10] M. D. Al-Tahat and A.-R. Abbas, "Activity-based cost estimation model for foundry systems producing steel castings.," *Jordan Journal of Mechanical and Industrial Engineering*, vol. 6, no. 1, 2012.

[11] Y. Liu, L. He, and S. Yuan, "Wear Properties of Aluminum Alloy 211z. 1 Drilling Tool.," *Jordan Journal of Mechanical and Industrial Engineering*, vol. 15, no. 1, 2021.

[12] R. N. Hwayyin and A. S. Ameed, "The Time Dependent Poisson's Ratio of Nonlinear Thermoviscoelastic Behavior of Glass/Polyester Composite.," *Jordan Journal of Mechanical and Industrial Engineering*, vol. 16, no. 4, 2022.

[13] N. S. RADHI, Z. AL-KHAFAJI, B. M. MAREAI, S. RADHI, and A. M. ALSAEGH, "REDUCING OIL PIPES CORROSION BY (ZN-NI) ALLOY COATING ON LOW CARBON STEEL SUBSTRATE BY SUSTAINABLE PROCESS," *Journal of Engineering Science and Technology*, vol. 18, no. 3, pp. 1624–1638, 2023.

[14] N. M. Dawood, N. S. Radhi, and Z. S. Al-Khafaji, "Investigation corrosion and wear behavior of Nickel-Nano silicon carbide on stainless steel 316L," in *Materials Science Forum*, Trans Tech Publ, 2020, pp. 33–43.

[15] N. S. Radhi and Z. Al-Khafaji, "Investigation biomedical corrosion of implant alloys in physiological environment," *International Journal of Mechanical and Production Engineering Research and Development*, vol. 8, no. 4, 2018, doi: 10.24247/ijmperdaug201827.

[16] N. M. Dawood, N. S. Radhi, and Z. S. Al-khafaji, "Investigation Corrosion and Wear Behavior of Nickel-Nano Silicon Carbide on Stainless Steel 316L," vol. 1002, pp. 33–43, 2020, doi: 10.4028/www.scientific.net/MSF.1002.33.

[17] N. S. Radhi, "Preparation and modeling (titanium-hydroxyapatite) functionally graded materials for bio-medical application," *International Journal of Civil Engineering and Technology*, vol. 9, no. 6, pp. 28–39, 2018.

[18] N. S. Radhi, H. H. Jamal Al-deen, R. Safaa Hadi, N. Al-Ghaban, and Z. S. Al-Khafaji, "Preparation And Investigation A Hydroxyapatite Layer Coating On Titanium Substrate For Surgical Implants.," *Journal of Nanostructures*, 2022.

[19] N. S. Radhi and Z. S. Al-Khafaji, "Preparation and Investigation composite coating (Ni-nano hydroxyapatite) on low carbon steel samples," in *6th International Scientific Conference on Nanotechnology, Advanced Materials and its Applications*, 2018. doi: 10.13140/RG.2.2.10097.79201.

[20] A. H. Haleem, N. S. Radhi, and N. T. Jaber, "A STUDY ON STAINLESS STEEL 316L UTILIZING SINGLE- STEP ANODIZATION AND A DC SPUTTERING PLASMA OF SILVER COATING TO IMPROVE CORROSION RESISTANCE," *Academic Journal of Manufacturing Engineering*, vol. 21, no. 4, pp. 1–10, 2023.

[21] N. S. Radhi, H. H. Jamal Al-deen, R. Safaa Hadi, nada Al-Ghaban, and Z. S. Al-Khafaji, "Preparation And Investigation A Hydroxyapatite Layer Coating On Titanium Substrate For Surgical Implants.," *Journal of Nanostructures*, 2023, [Online]. Available: https://jns.kashanu.ac.ir/article_113861.html

[22] M. A. Lieberman and A. J. Lichtenberg, "Principles of plasma discharges and materials processing. A John Wiley & Sons," *Inc., Hoboken, NJ, USA*, 2005.

[23] K. Hebbar Kannur, T. Bin Yaqub, C. Pupier, C. Héau, and A. Cavaleiro, "Mechanical properties and vacuum tribological performance of Mo–S–N sputtered coatings," *ACS Applied Materials & Interfaces*, vol. 12, no. 38, pp. 43299–43310, 2020.

[24] A. Ismail, R. Zenasni, K. S. M. Amine, and S. Ahmed, "Effect of tempering temperature on the mechanical properties and microstructure of low alloy steel DIN 41Cr4," *Jordan Journal of Mechanical and Industrial Engineering*, vol. 13, no. 1, pp. 9–14, 2019.

[25] H. J. Klasen, "Historical review of the use of silver in the treatment of burns. I. Early uses," *Burns*, vol. 26, no. 2, pp. 117–130, 2000.

[26] Y. Shen *et al.*, "Advances in Research on Titanium and Titanium Alloys with Antibacterial Functionality for Medical Use—A Review," *Journal of Biomaterials and Tissue Engineering*, vol. 13, no. 1, pp. 1–17, 2023.

[27] S. Srinivasan, P. T. Kumar, S. V Nair, S. V Nair, K. P. Chennazhi, and R. Jayakumar, "Antibacterial and bioactive α- and β-chitin hydrogel/nanobioactive glass ceramic/nano silver composite scaffolds for periodontal regeneration," *Journal of biomedical nanotechnology*, vol. 9, no. 11, pp. 1803–1816, 2013.

[28] E. Marsich *et al.*, "Biological responses of silver-coated thermosets: an in vitro and in vivo study," *Acta biomaterialia*, vol. 9, no. 2, pp. 5088–5099, 2013.

[29] M. Jabor, N. S. Radh, M. A. Al-Kinani, and Z. S. Al-Khafaji, "Optimization of Electro less of Nickel base coating for Cermet Cutting Tools Substrate".

[30] F. Yang, S. K. Both, X. Yang, X. F. Walboomers, and J. A. Jansen, "Development of an electrospun nano-apatite/PCL composite membrane for GTR/GBR application," *Acta biomaterialia*, vol. 5, no. 9, pp. 3295–3304, 2009.

[31] M. Herron *et al.*, "Reduction in wound bioburden using a silver-loaded dissolvable microfilm construct," *Advanced healthcare materials*, vol. 3, no. 6, pp. 916–928, 2014.

[32] B. M. Mareai, Z. S. Al-khafaji, and F. Al-husseinawi, "Bio-Medical Waste Management and Analysis for Selected Hospitals in Southern and middle parts of Iraq," *Waste forum*, vol. 2023, no. 1, pp. 58–68, 2023.

[33] H. A. Sallal, M. S. Radhi, M. H. Mahboba, and Z. Al-Khafaji, "Impact of embedded sol-gel synthesized triple composites on polymer's mechanical properties.," *Egyptian Journal of Chemistry*, 2022, doi: 10.21608/ejchem.2022.154630.6684.

[34] I. A. U. Kadhim, H. A. Sallal, and Z. S. Al-Khafaji, "A Review in Investigation of Marine Biopolymer (Chitosan) for Bioapplications," *ES Materials & Manufacturing*, vol. 21, 2023, doi: 10.30919/esmm5f828.

[35] E. Science *et al.*, "The Growing Importance of Hydroxyapatite in Modern Biomedicine (HAP): A Review of Recent Advances and Challenges," no. April, pp. 1–40, 2023.

[36] H. Singh, S. Singh, and C. Prakash, "Current trends in biomaterials and bio-manufacturing," *Biomanufacturing*, pp. 1–34, 2019.

[37] S. Dwivedi and S. Sharma, "Optimization of Resistance Spot Welding Process Parameters on Shear Tensile Strength of SAE 1010 steel sheets Joint using Box-Behnken Design.," *Jordan Journal of Mechanical and Industrial Engineering*, vol. 10, no. 2, 2016.